Pergamon

Int. J. Solids Structures Vol. 34, Nos 31–32, pp. 4237–4259, 1997

0020-7683/97 $17.00 + .00

PII: S0020-7683(96)00072-8

THICK-WALLED COMPOSITE BEAM THEORY INCLUDING 3-D ELASTIC EFFECTS AND TORSIONAL WARPING

CHEOL KIM and SCOTT R. WHITE
Department of Aeronautical and Astronautical Engineering, University of Illinois at Urbana-Champaign, Urbana, Illinois 61801, U.S.A.

(*Received* 22 *May* 1995; *in revised form* 28 *January* 1996)

Abstract—A composite box beam model is developed for both thin- and thick-walled composite beams. In this analysis primary and secondary torsional warping and transverse shear effects, both of the cross-section and of the beam walls, are considered. An efficient method to account for 3-dimensional elastic effects in laminated beam walls is developed. These non-classical effects are investigated and are shown to be accentuated as the wall thickness increases. The present theory is validated by comparison with available experimental data, other analytical results, and finite element analysis. Good correlation between the present theory and other results is achieved for all test cases with predictions within 10% of experimental data for thin-walled beams and 8% of 3-D FEA results for thick-walled cases. © 1997 Elsevier Science Ltd.

INTRODUCTION

Composite materials are finding increasing applications for thick primary load carrying structures subjected to high static and dynamic loadings, owing to innovative and cost-effective manufacturing technology. Many composite primary and secondary structural configurations such as aircraft wings, helicopter rotor blades, robot arms, bridges, and other structural elements in civil constructions can be idealized as thin- or thick-walled beams, leading to simpler governing equations.

Due to the inherent non-classical phenomena as large torsional warping and coupled deformations arising from the orthotropic or directional nature of fibrous composites, detailed structural models of composite thin- and thick-walled beams are essential in order to fully exploit special non-classical effects in design. In aeronautical applications for instance, emphasis is given to elastic tailoring of deformations which influence the aerodynamics of the composite structure, referred to as aeroelastic tailoring. In robot arm applications the design requirement is minimum endpoint deflection during articulating motion and fast setting time after actuation.

Mansfield and Sobey (1979) and Mansfield (1981) developed theories for composite one- or two-cell thin-walled cylindrical tubes and introduced the concepts of the aeroelastically tailored composite helicopter blade. Although they considered some coupling effects, they did not take into account transverse shear and cross-sectional warping in their models. Chang and Libove (1988) and Libove (1988) developed a simple theory for computing shear flows, cross-sectional normal stresses, and rate of twist in composite thin-walled beams of a single-cell closed cross-section. They assumed that the shape of the cross-section was preserved and the longitudinal strains varied linearly over the cross-section. No warping was included. A Vlasov-type theory for composite thin-walled beams with open cross sections was developed by Bauld and Tzeng (1984). The thin-walled beams considered were composed of a number of symmetric laminated plates. Wu and Sun (1992) developed a simplified theory for composite thin-walled beams. Under more general assumptions than those of Vlasov, the equilibrium equations consisted of seven ordinary differential equations. The effects of torsional warping and transverse shearing deformation, two dominant modes of deformation in composite thin-walled beams, were included.

Rehfield (1985) developed an appropriate theory used in a number of composite applications for thin-walled composite closed section beams. Two nonclassical effects,

elastic bending–shear coupling and restrained torsional warping, were investigated in some simple examples involving cantilevered thin-walled composite box beams using the theory by Rehfield *et al.* (1990). Berdichevsky (1982) formulated the geometrically nonlinear problem for an anisotropic rod based on the variational-asymptotical method by which the three-dimensional theory of elasticity solution can be split into two separate analyses: a nonlinear one-dimensional through-the-thickness analysis and a linear two-dimensional analysis. Atilgan *et al.* (1991) and Hodges *et al.* (1992) developed an asymptotically exact formulation for analysis of prismatic, nonhomogeneous, anisotropic beams based on geometrically nonlinear, three-dimensional elasticity. Since their model was restricted to very long beams, restrained warping effects were not considered. Cesnik *et al.* (1993) extended the above asymptotic theory for treatment of restrained warping. A variationally and asymptotically consistent theory was developed in order to derive the governing equations of anisotropic thin-walled beams with closed sections by Berdichevsky *et al.* (1992, 1993). This theory is based on a asymptotic analysis of two-dimensional shell theory and closed-form expressions for the beam-stiffness coefficients and stress–displacement relationships were found. Sutyrin and Hodges (1995) developed an asymptotically correct first-order shear deformation theory for laminated plates. Their numerical results showed improved accuracy compared to most first-order shear deformation theories. The potential energy method was used for formulating a thin-walled composite beam theory by Subrahmanyam (1993). When it was compared with experimental results, a good agreement was obtained for symmetric layup beams only.

Valuable experimental data on composite box beams were generated by Chandra *et al.* (1990). They fabricated symmetric and antisymmetric graphite/epoxy composite thin-walled box beams and tested under bending, torsional, and extensional loads. Smith and Chopra (1991) then refined this beam model by including transverse shear effects and a more exact form of the warping function. The theories of closed and open section beams were summarized in Chandra and Chopra (1992b). Chandra and Chopra (1992c) extended their single-cell theory to consider structural behavior of a two-cell composite beam. Chandra and Chopra (1992a) investigated the influence of elastic couplings on the free vibration characteristics of their thin-walled composite box beam model and correlated the results with experimental data.

Librescu and Song (1991) developed a refined theory for laminated composite thin-walled closed section beams of arbitrary cross-section that can account for the primary and secondary warpings. Free vibration and aeroelastic divergence analyses of aircraft wings modeled as composite beams were performed by Librescu and Song (1991), Librescu *et al.* (1993) and Song and Librescu (1993). This theory was modified for open cross-section beams later and a number of non-classical effects such as the transverse shear flexibility and warping restraint were studied in Song and Librescu (1993). As an example, the eigenvibration of composite I-beams was analyzed. Rand (1994) also performed a theoretical study of the free vibration characteristics of thin-walled composite blades which included out-of-plane warping.

None of these treatments are appropriate for composite thick-walled beams mainly due to their neglection of the shear stress variation across the thickness in developing a torsional warping function. This paper presents a beam model appropriate for both thin- and thick-walled geometries which includes coupled stiffness effects, transverse shear (of the cross-section and beam walls), and warping (primary and secondary).

THEORETICAL FORMULATION

Consider the slender elastic hollow rectangular composite beam shown in Fig. 1. The length of the beam is denoted by L, its horizontal wall thickness by h_h, its vertical wall thickness by h_v, the minimum cross-sectional dimension by c, and the maximum cross-sectional dimension by d. It is assumed that $d \ll L$ and no dimensional restrictions on the wall thickness h are imposed, distinguishing this treatment from a thin-walled theory. The Cartesian coordinate system (x, y, z) and the curvilinear coordinate system (x, s, n) are used in the present analysis. In this case, the origin of the Cartesian coordinates is set at the

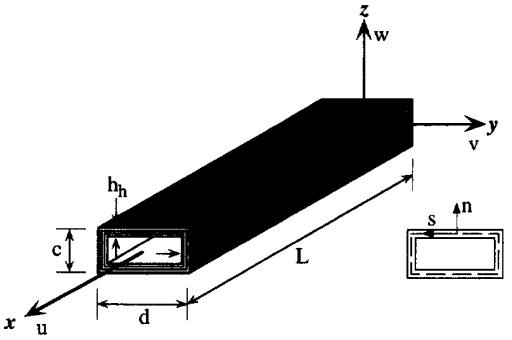

Fig. 1. Box beam geometry and coordinate directions.

center of the beam cross-section. The circumferential coordinate s is measured along the tangent to the middle surface in a counter-clockwise direction, whereas n is measured along the normal to the middle surface. The material is anisotropic and the elastic properties can vary circumferentially and in the direction normal to the middle surface.

Basic assumptions

A number of assumptions are adopted to model the slender beam as a single-cell thick-walled box beam with effective stiffnesses. A thick-walled beam is defined as a beam which satisfies $h_{max}/d \geqslant 0.1$, where h_{max} denotes the maximum thickness of the beam wall. The fundamental assumptions are:

(i) The contours of the original beam cross-sections do not deform in their own planes. This statement implies that the inplane deformation of the beam cross-section is neglected. This assumption is particularly valid as the wall thickness of the beam increases.

(ii) The out-of-plane displacement of the beam cross-section due to bending and shear is assumed to be described by a cubic function of the cross-sectional coordinates y or z (Levinson, 1981; Reddy, 1984). This means that transverse shear effects of the beam are considered and transverse shear strains vary parabolically across the thickness.

(iii) Any general beam wall segment behaves as a thick shell. This implies that the transverse shear effects of the wall segments are also taken into account.

(iv) Primary and secondary warping effects are taken into account. The warping displacement along the mid-line of the beam wall is referred to as primary warping and the warping of the cross-section normal to the mid-line contour is referred to as secondary warping.

Kinematic equations

The beam displacement fields may be expressed as

$$u(x,y,z) = u_o(x) - y\left[\phi_y(x) + \frac{4}{3}\left(\frac{y}{d}\right)^2 (v_o'(x) - \phi_y(x))\right] - z\left[\phi_z(x) + \frac{4}{3}\left(\frac{z}{c}\right)^2 (w_o'(x) - \phi_z(x))\right] - \left[\psi_p(y,z) + \psi_s(y,z)\right]\theta'(x) \tag{1a}$$

$$v(x,z) = v_o(x) - z\theta(x) \tag{1b}$$

$$w(x,y) = w_o(x) + y\theta(x) \tag{1c}$$

where the functions u, v, and w are x-, y-, and z-directional displacements, respectively. The

functions $u_o(x)$, $v_o(x)$ and $w_o(x)$ represent the rigid body translations along the x, y and z axes, while the variables $\phi_y(x)$ and $\phi_z(x)$ denote the rotations about the z and y axes and $\theta(x)$ is the angle of twist. The functions $\psi_p(y,z)$ and $\psi_s(y,z)$ denote the primary and secondary warping functions. The prime denotes differentiation with respect to x (i.e., $' = \mathrm{d}/\mathrm{d}x$), hereafter. The kinematic quantities $u_o(x)$, $v_o(x)$, $w_o(x)$, $\phi_y(x)$, $\phi_z(x)$ and $\theta(x)$ constitute the basic unknown functions of the problem.

The beam strain fields associated with the displacement fields are

$$\varepsilon_{xx} = \frac{\partial u}{\partial x} = u_o'(x) - y\left[\phi_y'(x) + \frac{4}{3}\left(\frac{y}{d}\right)^2 (v_o''(x) - \phi_y'(x))\right]$$

$$-z\left[\phi_z'(x) + \frac{4}{3}\left(\frac{z}{c}\right)^2 (w_o''(x) - \phi_z'(x))\right] - [\psi_p(y,z) + \psi_s(y,z)]\theta''(x)$$

$$\gamma_{xy} = \frac{\partial u}{\partial y} + \frac{\partial v}{\partial x} = \left(1 + 4\frac{y^2}{d^2}\right)(v_o'(x) - \phi_y(x)) - \left(z + \frac{\partial \psi}{\partial y}\right)\theta'(x) \tag{2b}$$

$$\gamma_{xz} = \frac{\partial u}{\partial z} + \frac{\partial w}{\partial x} = \left(1 + 4\frac{z^2}{c^2}\right)(w_o'(x) - \phi_z(x)) + \left(y - \frac{\partial \psi}{\partial z}\right)\theta'(x) \tag{2c}$$

in the vertical and horizontal walls of the box beam with $\psi = \psi_p + \psi_s$. From the assumed displacement fields in eqn (1) it can be readily seen that assumption (i) of cross-sectional nondeformability (implying $\varepsilon_{yy} = \varepsilon_{zz} = \gamma_{yz} = 0$) is satisfied.

Neglecting the shear stress variations across the thickness in developing a torsional warping function for composite beams may lead to erroneous results. This is because, as the thickness of a beam wall increases, the secondary warping effect becomes comparable in magnitude to that due to primary warping. Therefore, the torsional warping function derived from Bredt's assumptions is abandoned in this study. Instead, a torsional warping function which accounts for both primary and secondary warping effects simultaneously can be obtained by examining the theory of anisotropic solid beams. Here, the central portion of material whose boundary is a line of the constant stress function of the solid section is removed (Sokolnikoff, 1956). In this manner, the exact torsional warping function for a solid rectangular composite beam can be derived based on Lekhnitskii (1981) as,

$$\psi(y,z) = -yz + \frac{8a^2}{\mu\pi^3} \sum_{n=1,3,5,\ldots}^{\infty} \frac{1}{n^3} \frac{\sinh\dfrac{n\pi\mu}{d} z}{\cosh\dfrac{n\pi\mu}{2\xi}} \sin\frac{n\pi}{2} \sin\frac{n\pi y}{d} \tag{3}$$

where the central solid core of material is removed during the solution of the stiffness matrix integrals in the appendix. Here $\mu = \sqrt{G_{eh}/G_{ev}}$ and $\xi = d/c$ while G_{eh} and G_{ev} denote the effective shear moduli of horizontal and vertical walls. For isotropic materials the stiffness ratio $\mu = 1$ and this warping function reduces to the one presented in Sokolnikoff (1956).

Effective stiffness

The constitutive equations for the generally orthotropic kth layer can be written as

$$\begin{Bmatrix} \sigma_{xx} \\ \sigma_{ss} \\ \sigma_{nn} \\ \tau_{sn} \\ \tau_{nx} \\ \tau_{xs} \end{Bmatrix}_k = \begin{bmatrix} \bar{Q}_{11} & \bar{Q}_{12} & \bar{Q}_{13} & 0 & 0 & \bar{Q}_{16} \\ \bar{Q}_{12} & \bar{Q}_{22} & \bar{Q}_{23} & 0 & 0 & \bar{Q}_{26} \\ \bar{Q}_{13} & \bar{Q}_{23} & \bar{Q}_{33} & 0 & 0 & \bar{Q}_{36} \\ 0 & 0 & 0 & \bar{Q}_{44} & \bar{Q}_{45} & 0 \\ 0 & 0 & 0 & \bar{Q}_{45} & \bar{Q}_{55} & 0 \\ \bar{Q}_{16} & \bar{Q}_{26} & \bar{Q}_{36} & 0 & 0 & \bar{Q}_{66} \end{bmatrix}_k \begin{Bmatrix} \varepsilon_{xx} \\ \varepsilon_{ss} \\ \varepsilon_{nn} \\ \gamma_{sn} \\ \gamma_{nx} \\ \gamma_{xs} \end{Bmatrix}_k \tag{4}$$

where $\bar{Q}_{ij}$ are the transformed stiffnesses.

The anisotropic elastic characteristics of composite beam walls can result in highly three-dimensional elastic behavior. The specific manner in which the three-dimensional dependence in eqn (4) is accounted for in an equivalent one-dimensional beam theory is particularly important. It is quite reasonable in a one-dimensional beam theory that the off-cross-sectional stress components σ_{nn}, σ_{ss}, and τ_{sn} in eqn (4) are assumed to be negligibly small compared to the remaining stress components in the absence of internal or external pressure fields. However, the corresponding strains ε_{nn}, ε_{ss}, and γ_{sn} may not be negligibly small and are included in this formulation. For example, a significant through-the-thickness normal strain ε_{nn} can be generated in composite cylindrical shells for certain types of layups due to relatively large Poisson's ratios, ν_{xn} and ν_{sn} (Vinson, 1993).

By neglecting σ_{nn}, σ_{ss}, and τ_{sn}, the off-cross-sectional strain components can be expressed in terms of cross-sectional ones as,

$$\varepsilon_{ss} = B_1\varepsilon_{xx} + B_2\gamma_{xs} \tag{5a}$$

$$\varepsilon_{nn} = B_3\varepsilon_{xx} + B_4\gamma_{xs} \tag{5b}$$

$$\gamma_{sn} = B_5\gamma_{xn} \tag{5c}$$

where

$$B_1 = \frac{\bar{Q}_{13}\bar{Q}_{23} - \bar{Q}_{12}\bar{Q}_{33}}{\bar{Q}_{22}\bar{Q}_{33} - \bar{Q}_{23}^2} \tag{6a}$$

$$B_2 = \frac{\bar{Q}_{23}\bar{Q}_{36} - \bar{Q}_{26}\bar{Q}_{33}}{\bar{Q}_{22}\bar{Q}_{33} - \bar{Q}_{23}^2} \tag{6b}$$

$$B_3 = \frac{\bar{Q}_{12}\bar{Q}_{23} - \bar{Q}_{22}\bar{Q}_{13}}{\bar{Q}_{23}\bar{Q}_{33} - \bar{Q}_{23}^2} \tag{6c}$$

$$B_4 = \frac{\bar{Q}_{26}\bar{Q}_{23} - \bar{Q}_{22}\bar{Q}_{36}}{\bar{Q}_{22}\bar{Q}_{33} - \bar{Q}_{23}^2} \tag{6d}$$

$$B_5 = -\frac{\bar{Q}_{45}}{\bar{Q}_{44}}. \tag{6e}$$

Substituting eqns (5a–c) into the matrix expression (4) and keeping only the beam cross-sectional components, the reduced constitutive equations with three-dimensional elastic effects for the kth layer in the composite beam walls are expressed as

$$\begin{Bmatrix} \sigma_{xx} \\ \tau_{xs} \\ \tau_{nx} \end{Bmatrix}_k = \begin{bmatrix} C_{11} & C_{12} & 0 \\ C_{12} & C_{22} & 0 \\ 0 & 0 & C_{33} \end{bmatrix}_k \begin{Bmatrix} \varepsilon_{xx} \\ \gamma_{xs} \\ \gamma_{nx} \end{Bmatrix}_k \tag{7}$$

where

$$C_{11} = \bar{Q}_{11} + \frac{2\bar{Q}_{12}\bar{Q}_{13}\bar{Q}_{23} - \bar{Q}_{12}^2\bar{Q}_{33} - \bar{Q}_{13}^2\bar{Q}_{22}}{\bar{Q}_{22}\bar{Q}_{33} - \bar{Q}_{23}^2} \tag{8a}$$

$$C_{12} = \bar{Q}_{16} + \frac{\bar{Q}_{12}\bar{Q}_{23}\bar{Q}_{36} - \bar{Q}_{12}\bar{Q}_{26}\bar{Q}_{33} + \bar{Q}_{13}\bar{Q}_{23}\bar{Q}_{26} - \bar{Q}_{13}\bar{Q}_{22}\bar{Q}_{36}}{\bar{Q}_{22}\bar{Q}_{33} - \bar{Q}_{23}^2} \tag{8b}$$

$$C_{22} = \bar{Q}_{66} + \frac{2\bar{Q}_{23}\bar{Q}_{26}\bar{Q}_{36} - \bar{Q}_{26}^2\bar{Q}_{33} - \bar{Q}_{36}^2\bar{Q}_{22}}{\bar{Q}_{22}\bar{Q}_{33} - \bar{Q}_{23}^2} \tag{8c}$$

$$C_{33} = \bar{Q}_{55} - \frac{\bar{Q}_{45}^2}{\bar{Q}_{44}}. \tag{8d}$$

For instance, the reduced constitutive equation for the horizontal walls is obtained by replacing the subscripts s and n in eqn (8) by y and z, respectively,

$$\begin{Bmatrix} \sigma_{xx} \\ \tau_{xy} \\ \tau_{zx} \end{Bmatrix}_k = \begin{bmatrix} C_{11} & C_{12} & 0 \\ C_{12} & C_{22} & 0 \\ 0 & 0 & C_{33} \end{bmatrix}_k \begin{Bmatrix} \varepsilon_{xx} \\ \gamma_{xy} \\ \gamma_{zx} \end{Bmatrix}_k. \tag{9}$$

Analogously, in the vertical walls the relations are obtained by replacing the subscripts s and n in eqn (8) by z and y, respectively. By substituting the strain–displacement relations into the stress–strain relations, the stresses within the beam walls can be expressed in terms of the displacement functions of the beam cross-section.

The effective shear modulus G_e in eqn (3) can be determined from eqns (7) and (8). The laminate resultant forces are related to the strains as

$$\begin{Bmatrix} N_{xx} \\ N_{xs} \\ N_{nx} \end{Bmatrix} = \begin{bmatrix} D_{11} & D_{12} & 0 \\ D_{12} & D_{22} & 0 \\ 0 & 0 & D_{33} \end{bmatrix} \begin{Bmatrix} \varepsilon_{xx} \\ \varepsilon_{xs} \\ \varepsilon_{nx} \end{Bmatrix} \tag{10}$$

where $D_{ij} = \Sigma_{n=1}^{\#\text{ofplies}} C_{ij}^{(n)} t_{ply}^{(n)}$ and t_{ply} denotes one ply thickness. Assuming that a pure torque is applied to a beam, then N_{xx} is zero and ε_{xx} can be expressed in terms of ε_{xs}. As a result, G_e is obtained as

$$G_e = \frac{1}{h}\left(\frac{N_{xs}}{\varepsilon_{xs}}\right) = \frac{1}{h}\left(D_{22} - \frac{D_{12}^2}{D_{11}}\right). \tag{11}$$

Equilibrium equations

The generalized resultant forces and moments acting over the cross-section can be related to the stresses in the beam walls by equilibrium in the global coordinate system as

$$F(x) = \int_z \int_y \sigma_{xx}\, dy\, dz \tag{12a}$$

$$V_y(x) = \int_z \int_y \tau_{xy}\, dy\, dz \tag{12b}$$

$$V_z(x) = \int_z \int_y \tau_{xz}\, dy\, dz \tag{12c}$$

$$T(x) = \int_z \int_y \left[\left(y - \frac{\partial \psi}{\partial z}\right)\tau_{xz} - \left(z + \frac{\partial \psi}{\partial y}\right)\tau_{xy}\right] dy\, dz + \frac{\partial}{\partial x}\int_z \int_y \psi \sigma_{xx}\, dy\, dz \tag{12d}$$

$$M_y(x) = -\int_z \int_y \sigma_{xx} z\, dy\, dz \tag{12e}$$

$$M_z(x) = -\int_z \int_y \sigma_{xx} y\, dy\, dz \tag{12f}$$

where $F(x)$, $V_y(x)$, and $V_z(x)$ denote the axial force and the shear forces in the x, y, and z directions, respectively, while $T(x)$, $M_y(x)$, and $M_z(x)$ denote the moments about the x, y, and z axes. The torsional equilibrium relations, which include the torsional warping effects on the beam cross-section, were originally derived by Brunelle (1972).

Since anisotropic shear center locations depend on material parameters as well as section geometry, the shear center position may not lie on the geometric axes of symmetry. This means that the shear force acting on the geometric axes of symmetry may result in an

additional resultant torque. However, an analysis by Pollock *et al.* (1994) shows that the effect of material parameters on the shear center deviation from the geometric axes of symmetry is negligibly small for closed section beams. Therefore, $T(x)$ does not include the effect of shear center deviation due to material parameters.

Force-displacement relations

The governing equations for three types of specially tailored layups with specialized elastic couplings are considered in this paper. These include the cross-ply layup configuration, the circumferentially asymmetric stiffness (CAS) configuration, and the circumferentially uniform stiffness (CUS) configuration. The names CAS and CUS were adopted by Rehfield *et al.* (1990). The CAS configuration is also known as the symmetric configuration and the CUS configuration as the antisymmetric configuration by Chandra *et al.* (1990) and Smith and Chopra (1991).

The CAS configuration produces a bending-twist coupling so that an applied bending moment or torque produces a coupled deflection and twisting. The governing equations are expressed in matrix form as

$$\begin{Bmatrix} F(x) \\ V_y(x) \\ V_z(x) \end{Bmatrix} = \begin{bmatrix} K_{11} & K_{12} & K_{13} \\ K_{21} & K_{22} & 0 \\ K_{31} & 0 & K_{33} \end{bmatrix} \begin{Bmatrix} u_o'(x) \\ v_o'(x) - \phi_y(x) \\ w_o'(x) - \phi_z(x) \end{Bmatrix} \tag{13a}$$

$$\begin{Bmatrix} T(x) \\ M_y(x) \\ M_z(x) \end{Bmatrix} = \begin{bmatrix} K_{44} & K_{45} & K_{46} \\ K_{54} & K_{55} & 0 \\ K_{64} & 0 & K_{66} \end{bmatrix} \begin{Bmatrix} \theta'(x) \\ \phi_z'(x) \\ \phi_y'(x) \end{Bmatrix} \tag{13b}$$

where K_{ij} terms are the beam effective stiffnesses, similar to EA, EI, and GJ terms for the isotropic beam theory, and can be determined by integrating the equilibrium equations. These terms are written explicitly in the appendix. For the cross-ply layup configuration, fibers are aligned at 0° or 90° with respect to the beam spanwise axis so that no elastic couplings exist. This is a special case of the CAS configuration so that its governing eqn (13) reduces to one with only diagonal beam stiffnesses.

The CUS configuration produces extension-twist coupling so that an applied axial force or torque generates coupled beam extension and twisting. The governing equations in this case are,

$$\begin{Bmatrix} F(x) \\ T(x) \end{Bmatrix} = \begin{bmatrix} K_{11} & K_{14} \\ K_{41} & K_{44} \end{bmatrix} \begin{Bmatrix} u_o'(x) \\ \theta'(x) \end{Bmatrix} \tag{14a}$$

$$\begin{Bmatrix} V_y(x) \\ V_z(x) \\ M_z(x) \\ M_y(x) \end{Bmatrix} = \begin{bmatrix} K_{22} & 0 & 0 & K_{25} \\ 0 & K_{33} & K_{36} & 0 \\ 0 & K_{63} & K_{66} & 0 \\ K_{52} & 0 & 0 & K_{55} \end{bmatrix} \begin{Bmatrix} v_o'(x) - \phi_y(x) \\ w_o'(x) - \phi_z(x) \\ \phi_y'(x) \\ \phi_z'(x) \end{Bmatrix}. \tag{14b}$$

Based on the governing eqn (13 or 14) and in conjunction with appropriate boundary conditions, the deformations of thin- or thick-walled composite beams can be determined when the applied forces and moments are specified. Numerical integration was performed ply by ply to obtain K_{ij} in this study. Once, these were obtained a simple matrix inversion was performed to obtain explicit relations for the displacements u_o, v_o, w_o and rotations θ, ϕ_y, and ϕ_z.

Table 1. Mechanical properties of AS4/3501-6

$E_{11} = 141.96$ Gpa	$E_{22} = E_{33} = 9.79$ GPa
$G_{12} = G_{13} = 6.0$ GPa	$G_{23} = 4.83$ GPa
$\nu_{12} = \nu_{13} = 0.24$	$\nu_{23} = 0.5$

Table 2. Thin- and thick-walled box beam geometry

Parameters	Thin beam (cross-ply)	Thin beam (CAS&CUS)	Thick beam (CAS&CUS)
L, Length (mm)	762.0	762.0	1,524.0
d, Outer width (mm)	52.3	24.2	106.7
c, Outer depth (mm)	26.0	13.6	50.8
L/d, Slenderness ratio	14.5	31.5	14.3
h, Wall thickness (mm)	0.762	0.762	15.24
Number of layers	6	6	120
Layer thickness (mm)	0.127	0.127	0.127

APPLICATIONS

The present theory is used to predict the behavior of cantilevered thin- and thick-walled box beams made of AS4/3501-6 graphite/epoxy subjected to several types of loadings and comparisons are made with experimental data (Chandra *et al.*, 1990), refined beam FEA results (Stemple and Lee, 1988), other analytical predictions (Smith and Chopra, 1991), and 3-D FEA results. A similar analysis was also performed for cantilevered thin- and thick-walled circular beams and a good agreement was obtained between the analysis, experimental results, and 3-D FEA results (Kim and White, 1996). The mechanical properties of AS4/3501-6 are listed in Table 1. The geometric dimensions of the thin- and thick-walled box beams are tabulated in Table 2.

Thin-walled box beam

For the cross-ply configuration, the bending slope under a tip shear load of 4.45 N in the z direction and the twist angle under a tip torque of 11.3N·cm are calculated and shown in Fig. 2 and 3 along with other analytical results. It is interesting to note that there are only small discrepancies among the three analytical results in the two figures, even though the present theory adopts more rigorous methods to capture non-classical effects. This indicates that the effects of shear and torsional warping are quite small for this uncoupled configuration. Results show that good correlation exists between the present theory and experimental data.

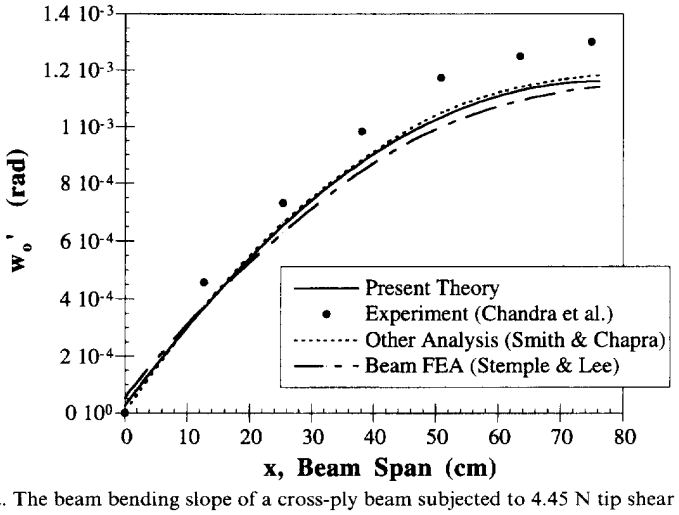

Fig. 2. The beam bending slope of a cross-ply beam subjected to 4.45 N tip shear load.

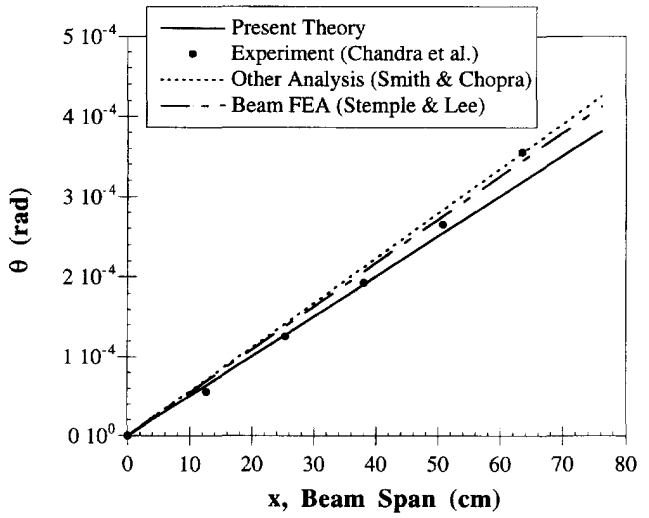

Fig. 3. The twist angle of a cross-ply beam subjected to 0.113 N-m tip torque.

Table 3. Thin-walled box beam layups

	Flanges		Webs	
Layup	Top	Bottom	Left	Right
Cross-ply	$[0/90]_3$	$[0/90]_3$	$[0/90]_3$	$[0/90]_3$
CAS1	$[15]_6$	$[15]_6$	$[15/-15]_3$	$[15/-15]_3$
CAS2	$[30]_6$	$[30]_6$	$[30/-30]_3$	$[30/-30]_3$
CAS3	$[45]_6$	$[45]_6$	$[45/-45]_3$	$[45/-45]_3$
CUS1	$[15]_6$	$[-15]_6$	$[15]_6$	$[-15]_6$
CUS2	$[0/30]_3$	$[0/-30]_3$	$[0/30]_3$	$[0/-30]_3$
CUS3	$[0/45]_3$	$[0/-45]_5$	$[0/45]_3$	$[0/-45]_3$

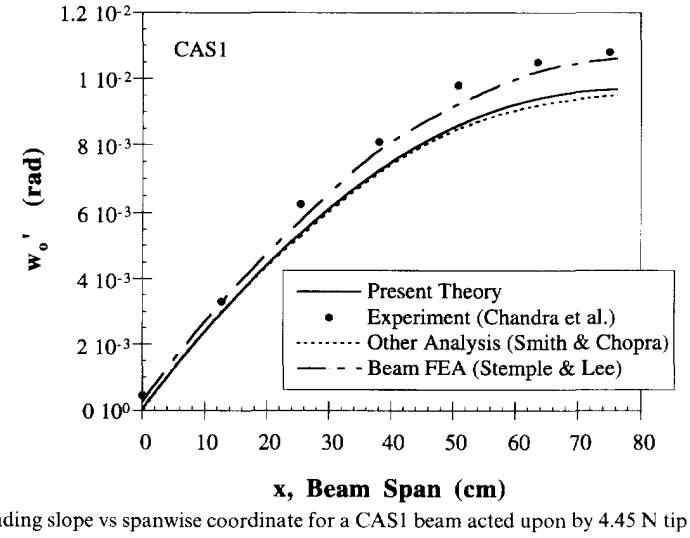

Fig. 4. Bending slope vs spanwise coordinate for a CAS1 beam acted upon by 4.45 N tip shear load.

For the CAS configuration, the bending slopes of three layup cases were calculated under 4.45 N tip shear load (see Table 3). The present results agree with experimental data within 10% as shown in Figs 4–6. Notably, the bending-induced twist responses of all test cases show excellent agreement in Figs 7–9. This indicates the rigorous methods to account for shear and torsional warping effects (primary and secondary warpings) in the present

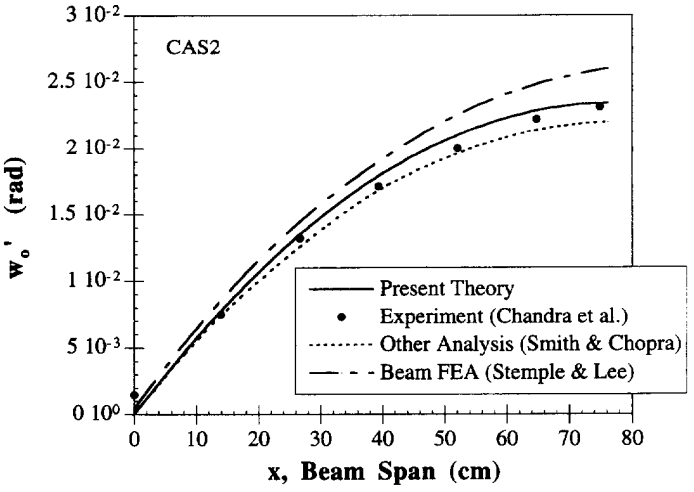

Fig. 5. Bending slope vs spanwise coordinate for a CAS2 beam acted upon by 4.45 N tip shear load.

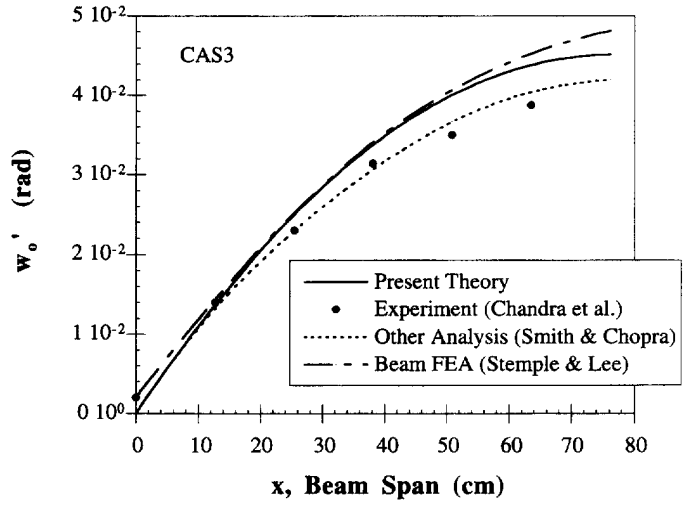

Fig. 6. Bending slope vs spanwise coordinate for a CAS3 beam acted upon by 4.45 N tip shear load.

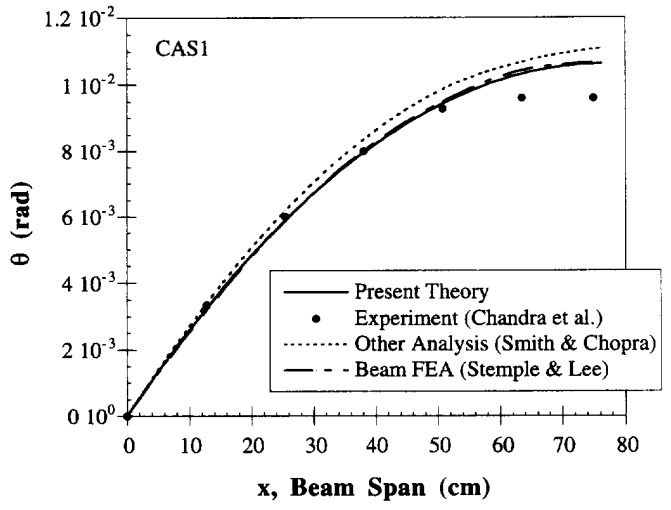

Fig. 7. Twist angle vs spanwise coordinate for a CAS1 beam acted upon by 4.45 N tip shear load.

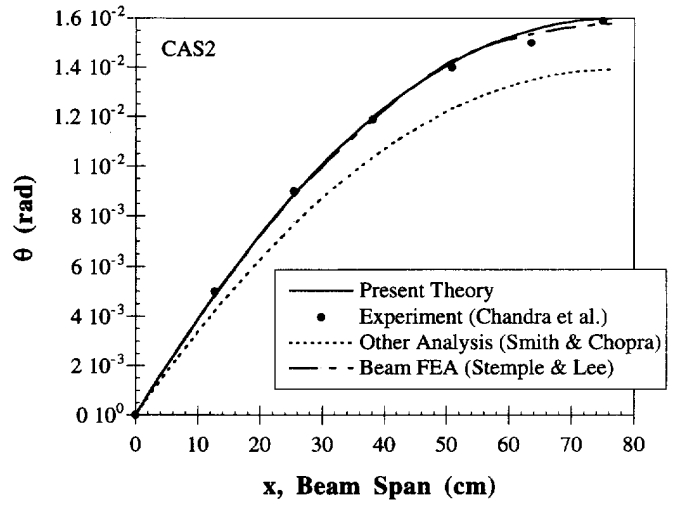

Fig. 8. Twist angle vs spanwise coordinate for a CAS2 beam acted upon by 4.45 N tip shear load.

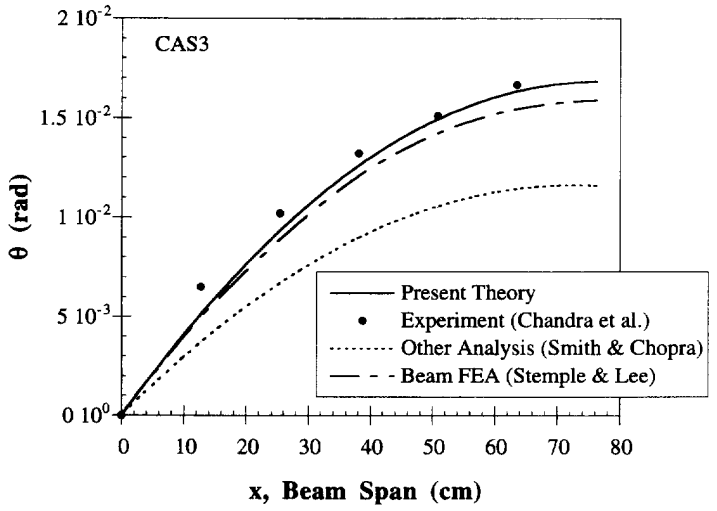

Fig. 9. Twist angle vs spanwise coordinate for a CAS3 beam acted upon by 4.45 N tip shear load.

formulation is quite effective. In particular, the present approach to account for 3-dimensional beam stiffness effects seems to play a major role in improving the predictions compared to the other analytical model of Smith and Chopra (1991) in which only in-plane stiffness coefficients and primary warping were considered. The secondary warping for thin-walled beams is known to be quite small. Further justification for this observation is evident from the CAS results. As the layup angle is increased, the difference between the other analytical results and experimental data increases and reaches a maximum for the $[45]_6$ layup case (CAS3) in which transverse shear effects are dominant.

The correlation between the predicted beam responses and experiments under 11.3 N·cm tip torque is generally excellent as shown in Figs 10–12. This again indicates that the rigorous methods to capture shear and warping effects in the present theory are quite effective for accurately predicting beam torsional responses. It is well known that the shear and warping effects are closely related to torsional responses. On the other hand, the differences between the other analytical results and experimental data increased and reached a maximum for a $[45]_6$ layup case again, as a layup angle increased. Torsion-induced bending slopes were calculated for all three cases with good agreement between the present results and experimental data. An illustration for the CAS3 case is shown in Fig. 13. It is also clear that in these cases the coupling effects, the magnitudes of torsion-induced bending slopes, are significant compared to torsion-induced twist angles.

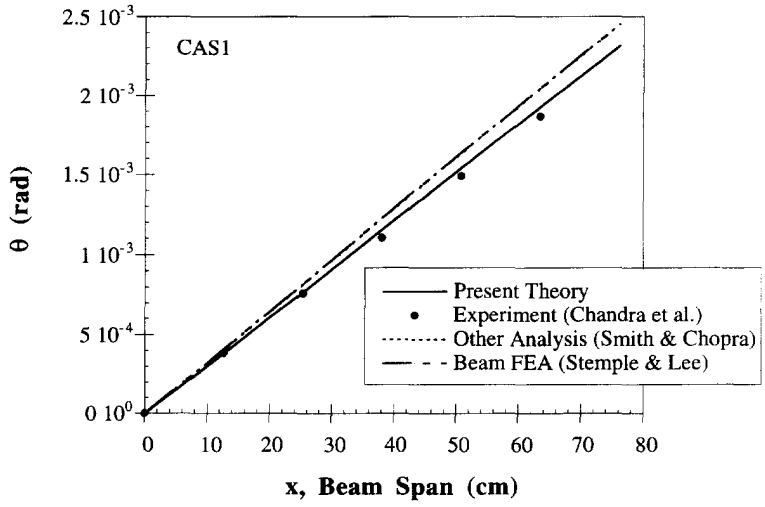

Fig. 10. Twist angle vs spanwise coordinate for a CAS1 beam acted upon by 0.113 N-m tip torque.

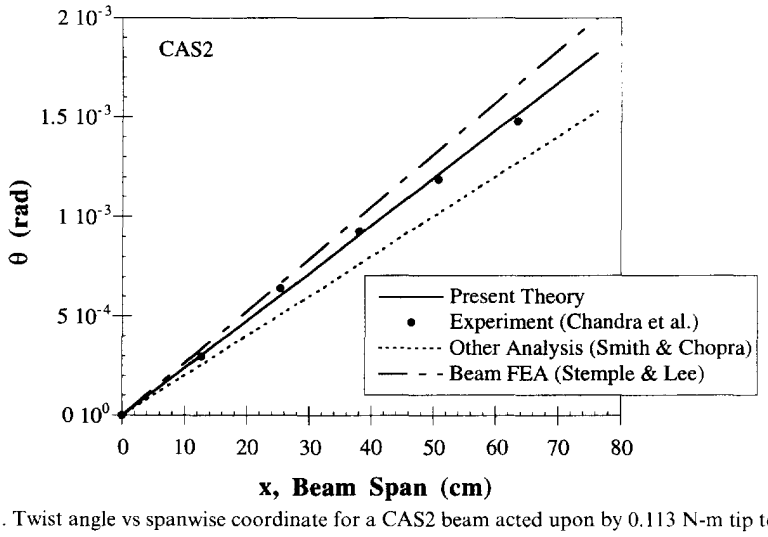

Fig. 11. Twist angle vs spanwise coordinate for a CAS2 beam acted upon by 0.113 N-m tip torque.

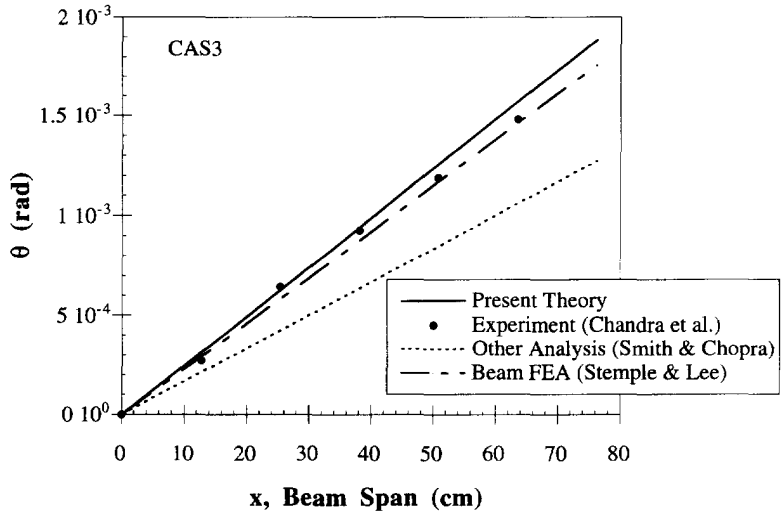

Fig. 12. Twist angle vs spanwise coordinate for a CAS3 beam acted upon by 0.113 N-m tip torque.

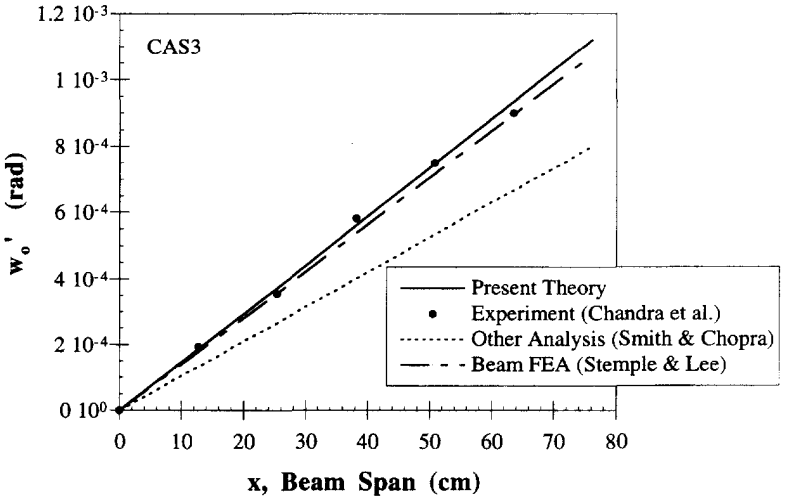

Fig. 13. Bending slope vs spanwise coordinate for a CAS3 beam acted upon by 0.113 N-m tip torque.

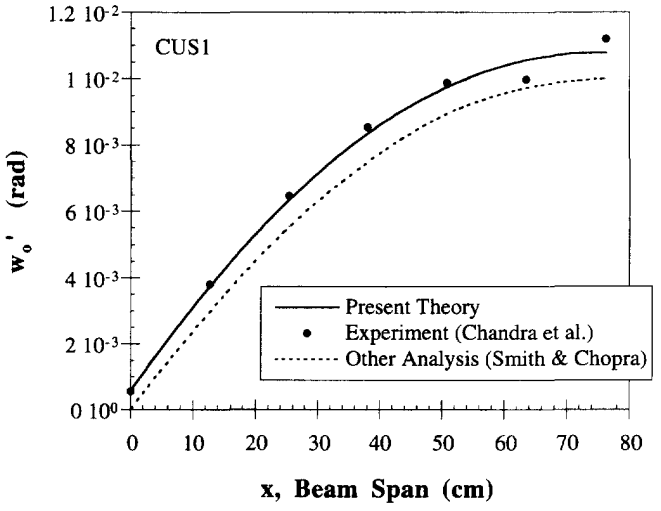

Fig. 14. Bending slope vs spanwise coordinate for a CUS1 beam acted upon by 4.45 N tip shear load.

Finally, the CUS configuration was considered under two types of loadings—tip shear, and tip torsional loads. In Figs 14 and 15, the bending slope of CUS1 and CUS3 cantilevered beams subjected to 4.45 N transverse tip load is plotted against the spanwise coordinate. It is interesting to note the bending slope is non-zero at the root. The bending-transverse shear coupling effect is relatively large for this configuration. The large transverse shear effect for this configuration was also noticed in Smith and Chopra (1991). The correlations of the present predictions with the experimental results are quite good for both cases. Figures 16–18 show the twist angle variation along the spanwise coordinate for the three CUS beams subjected to a tip torque of 11.3 N·cm. For these cases, no other analytical or finite element results could be found. Under pure torsional loading, the CUS3 configuration shows the best correlation. The results for the other CUS configurations are within 11% of experimental data.

For thin-walled composite box beams, the predictions of the present theory are as good as or better than those of either refined beam FEA or the other analytical formulations for all cases examined.

Thick-walled box beam

Three different layups of CAS and CUS beams were investigated and the specific layup sequences are listed in Table 4. The ratio of thickness to width is 0.14 ($\geqslant 0.1$). For each

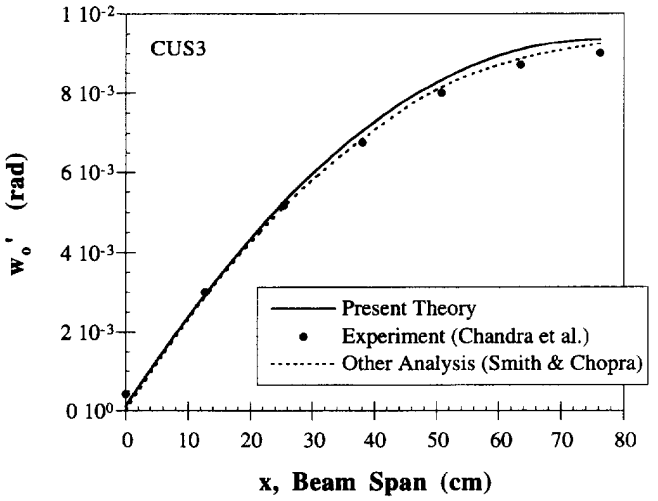

Fig. 15. Bending slope vs spanwise coordinate for a CUS3 beam acted upon by 4.45 N tip shear load.

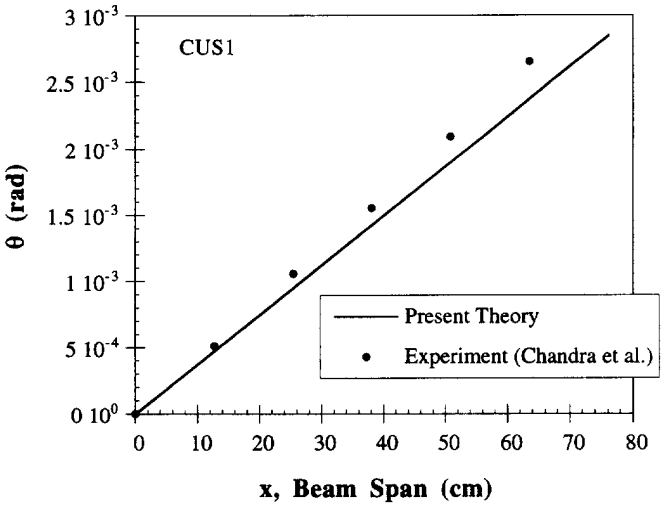

Fig. 16. Twist angle vs spanwise coordinate for a CUS1 beam acted upon by 0.113 N-m tip torque.

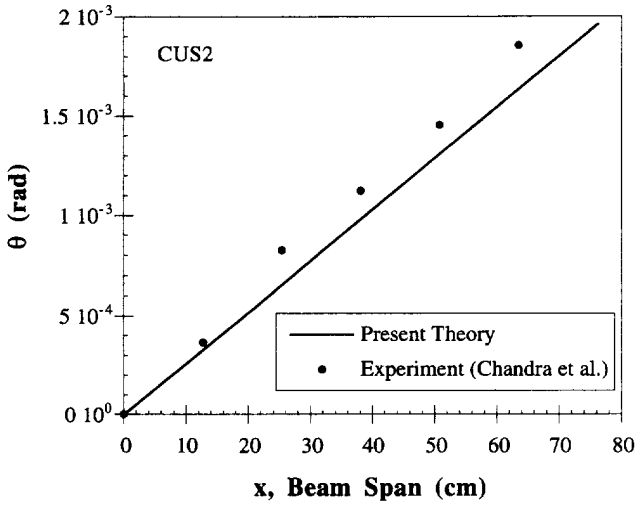

Fig. 17. Twist angle vs spanwise coordinate for a CUS2 beam acted upon by 0.113 N-m tip torque.

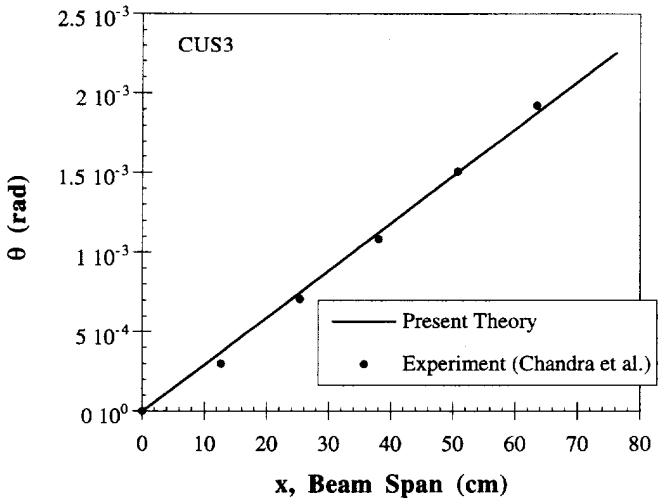

Fig. 18. Twist angle vs spanwise coordinate for CUS3 beam acted upon by 0.113 N-m tip torque.

Table 4. Thick-walled box beam layups

	Flanges		Webs	
Layup	Top	Bottom	Left	Right
CAS4	$[15_{20}/-15_{20}]_3$	$[15_{20}/-15_{20}]_3$	$[15]_{120}$	$[15]_{120}$
CAS5	$[30_{20}/-30_{20}]_3$	$[30_{20}/-30_{20}]_3$	$[30]_{120}$	$[30]_{120}$
CAS6	$[45_{20}/-45_{20}]_3$	$[45_{20}/-45_{20}]_3$	$[45]_{120}$	$[45]_{120}$
CUS4	$[0_{20}/15_{20}]_3$	$[0_{20}/-15_{20}]_3$	$[15]_{120}$	$[15]_{120}$
CUS5	$[0_{20}/30_{20}]_3$	$[0_{20}/-30_{20}]_3$	$[30]_{120}$	$[30]_{120}$
CUS6	$[0_{20}/45_{20}]_3$	$[0_{20}/-45_{20}]_3$	$[45]_{120}$	$[45]_{120}$

case, beams were subjected to two different types of loadings (a tip shear load of 4.45 kN and a tip torque of 1.13 kN·m). Deformations along the beam span were calculated for the six layup cases by the present analytical theory and compared to three-dimensional FEA results.

The thick-walled composite box beams were modeled using ABAQUS (C3D8R element) with six elements through the flange thickness and one element through the web thickness. The anisotropic material behavior of the composite beam precludes any symmetry assumptions, hence the entire structure is discretized. A total of 21,228 degrees of freedom, 7,076 nodes, and 5,280 elements were used to discretize each beam. Special care was taken in the application of consistent loading so that statically equivalent tip shear force and torque were applied. For the tip shear loading case, the vertical forces are distributed over all free end nodes in a parabolic fashion. This yields zero shear stress at the top and bottom of the end section with the resultant force equaling the applied shear load. For the tip torque case, shear forces are distributed on all free end nodes in the cross-sectional coordinates (y and z) so-as to yield a linear shear stress distribution over the free end section with zero shear resultant.

In Fig. 19, the transverse deflections of CAS beams subjected to 4.45 kN transverse tip load are plotted against the spanwise coordinate. The predictions by the present theory are overlayed with the 3-D FEA results. The correlation between the two results is excellent. Figure 20 shows the bending-induced twist distributions for these cases. Again, the correlation is excellent. This indicates that the present method of accounting for 3-D elastic effects and torsional warping is sufficient to describe the coupled deformational behavior of thick-walled composite beams. The results for CUS box beams subjected to a 1.13 kN·m

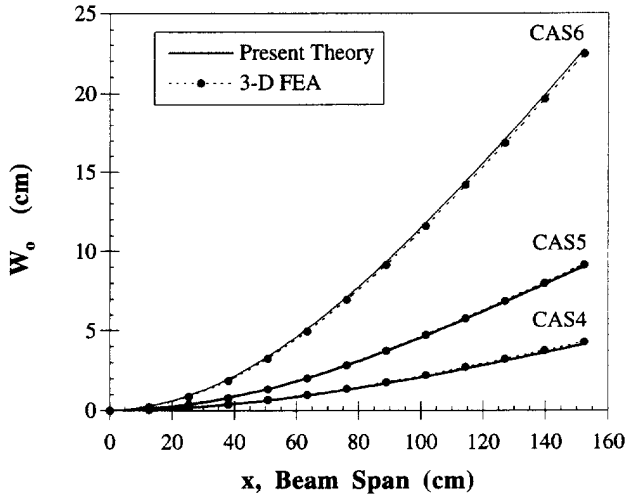

Fig. 19. Transverse deflection vs spanwise coordinate for CAS beams acted upon by 4.45 kN tip shear load.

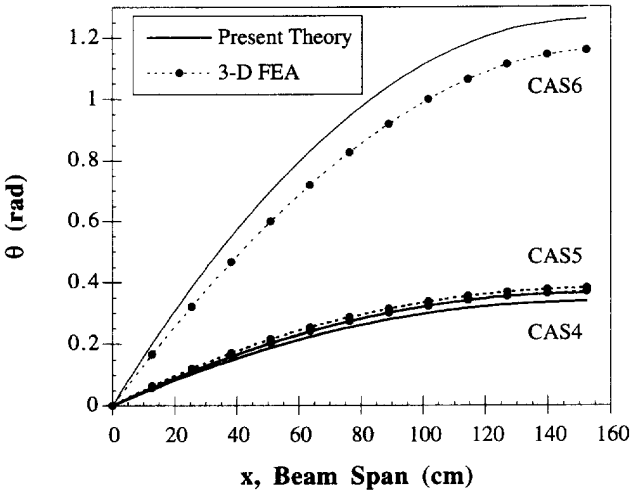

Fig. 20. Twist angle vs spanwise coordinate for CAS beams acted upon by 4.45 kN tip shear load.

tip torque are shown in Figs 21 and 22. In Fig. 21, only a representative twisting response for CUS4 is shown. Correlation is excellent for all cases.

INVESTIGATIONS OF IMPORTANT EFFECTS

Beams composed of anisotropic materials show many types of non-classical effects compared to isotropic beams. Thus, the accuracy of an anisotropic beam theory strongly depends on the approach used to account for these non-classical effects. In formulating the present theory several rigorous methods were used to capture such effects and we now assess their contributions to the elastic response of composite beams.

Three-dimensional elastic effect

Adequate treatment of three-dimensional elastic properties within walls composed of laminated plies is very important in the analysis of composite hollow beams since elastic properties in composite beam walls vary significantly with ply orientation angle. For certain types of layups, mismatch of Poisson's effect between plies is so significant that it causes

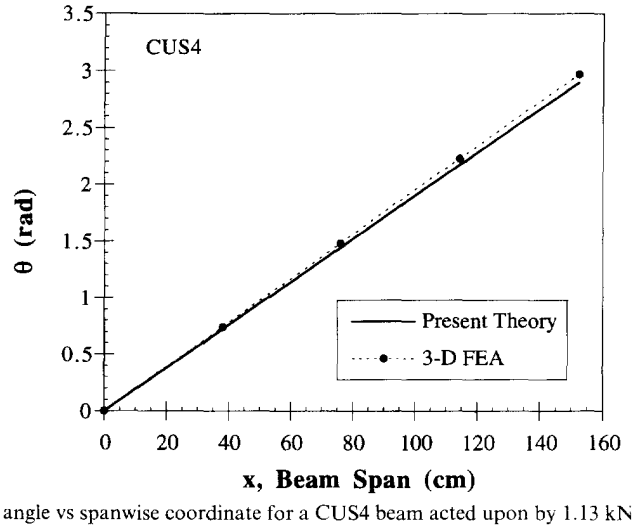

Fig. 21. Twist angle vs spanwise coordinate for a CUS4 beam acted upon by 1.13 kN-m tip torque.

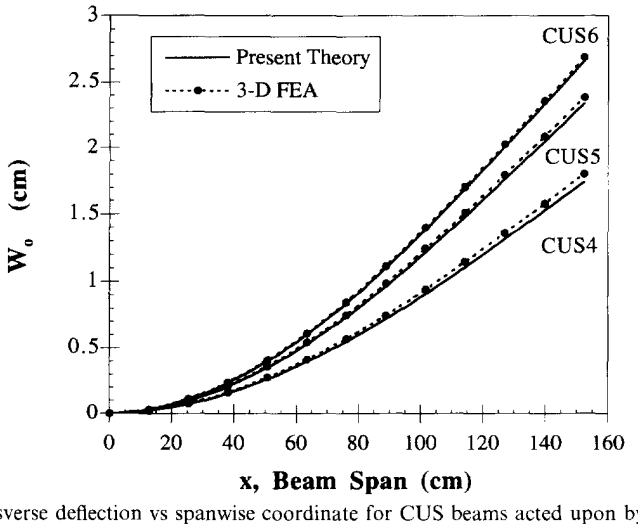

Fig. 22. Transverse deflection vs spanwise coordinate for CUS beams acted upon by 4.45 kN tip shear load.

the beam walls to behave in a highly three-dimensional elastic fashion. The present theory considers all three-dimensional ply stiffness coefficients, including all shear and normal components. The resulting beam stiffness is denoted as 3-D stiffness hereafter. On the other hand, beam stiffnesses considering only the inplane components of ply stiffness coefficients will be denoted as 2-D stiffness. The 2-D stiffness is widely used in most composite thin-walled beam theories.

The influence of the 3-D effects on the elastic response of composite box beams is assessed by predicting deformations using both 2-D and 3-D stiffnesses. The same warping function (primary and secondary warping) is used for both cases. Figure 23 shows the twist distributions predicted using both approaches for the CAS3 beam (6 ply-thick) subjected to 4.45 N tip transverse shear load together with experimental results. The difference between the 3-D and 2-D stiffness results is significant (23%) for this layup configuration. The predictions with 3-D stiffness formulation is quite close to the experimental data, while the predictions with 2-D stiffnesses closely resembles Smith and Chopra (1991). Figure 24 shows the twist distribution predictions using both approaches for the CUS3 beam (6 plies-thick) subjected to 4.45 N tip extensional load together with experimental verification. Again, the twist values using the 3-D stiffness formulation agree more closely with experimental data.

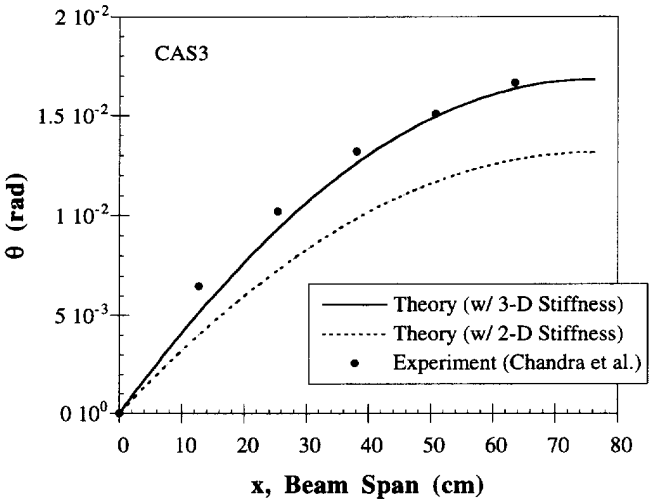

Fig. 23. 3-D stiffness effects on bending-induced twist for a CAS3 beam acted upon by 4.45 N tip shear load.

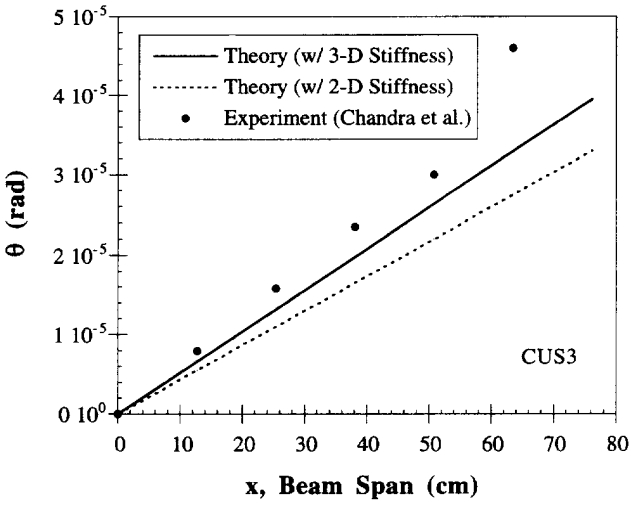

Fig. 24. 3-D stiffness effects on extension-induced twist for a CUS3 beam acted upon by 4.45 N tip extension load.

The above results clearly demonstrate that the 3-D stiffness formulation which accounts for all ply shear properties significantly improves the predictions of beam twisting deformations inherently governed by shear stresses without changing the accuracy of the present theory in predicting bending deformations.

Torsional warping effect

Torsional warping has significant effects on torsional and coupled torsional deformations of composite box beams. The present theory accounts for both torsional primary and secondary warpings, so it is valuable to assess the effect of each warping on the overall behavior of elastically tailored box beams. In the following results, the 3-D stiffness formulation has been used for all cases and deformations considering only primary warping are isolated from results with both primary and secondary warping.

Figures 25 and 26 show bending and coupled twist deformations of a CAS2 beam subjected to 4.45 N tip shear load. The effects of thickness (secondary) warping is very small for this thin-walled beam. Figures 27 and 28 show bending and coupled twist deformations of a thick CAS5 beam subjected to 4.45 kN tip shear load. The bending deformations are all quite close indicating that the contribution of secondary warping to beam bending response is small even for a thick-wall composite beam under bending load. On

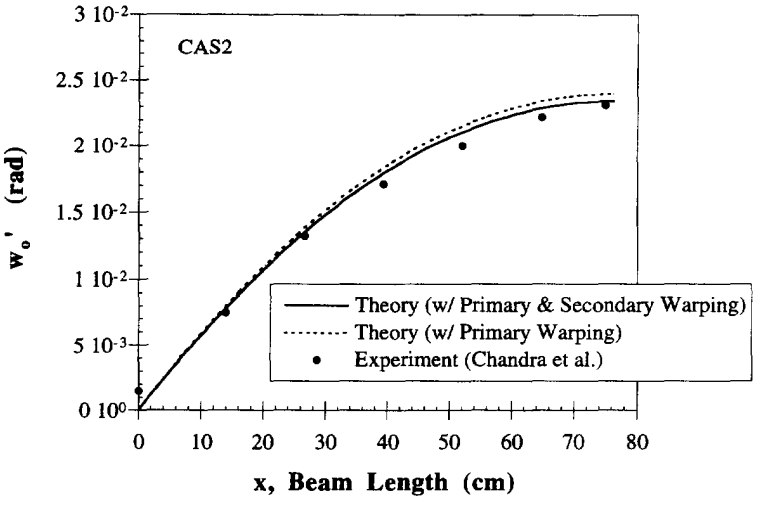

Fig. 25. Secondary warping effect on bending for a CAS2 beam acted upon by 4.45 N tip shear load.

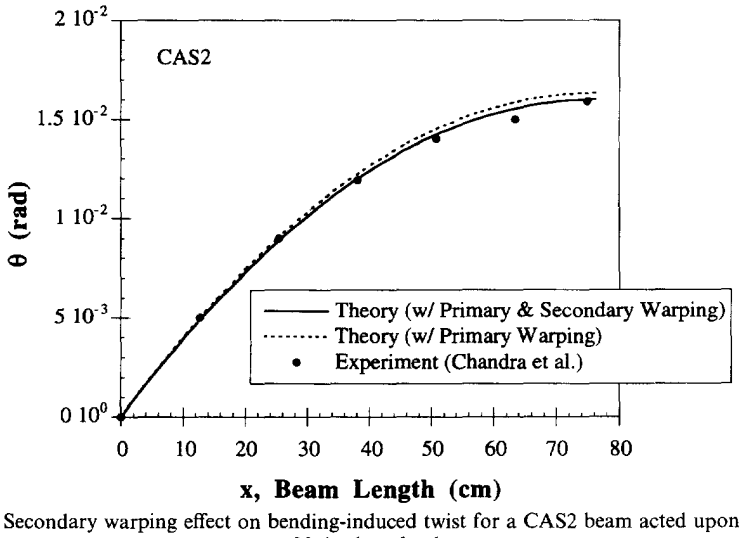

Fig. 26. Secondary warping effect on bending-induced twist for a CAS2 beam acted upon by 4.45 N tip shear load.

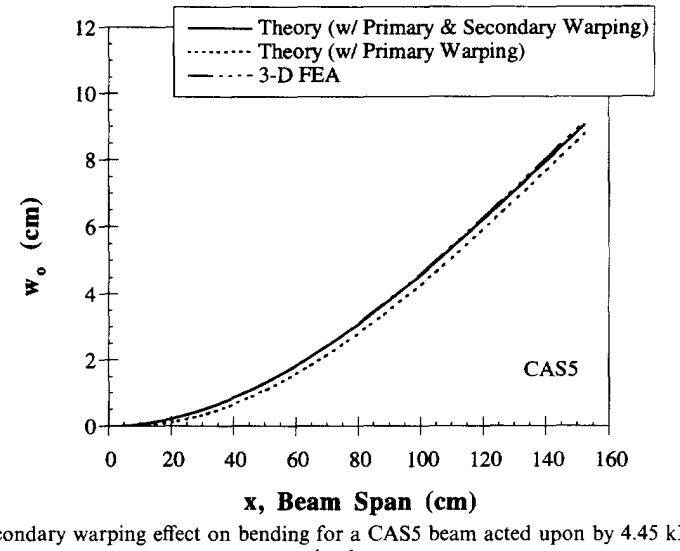

Fig. 27. Secondary warping effect on bending for a CAS5 beam acted upon by 4.45 kN tip shear load.

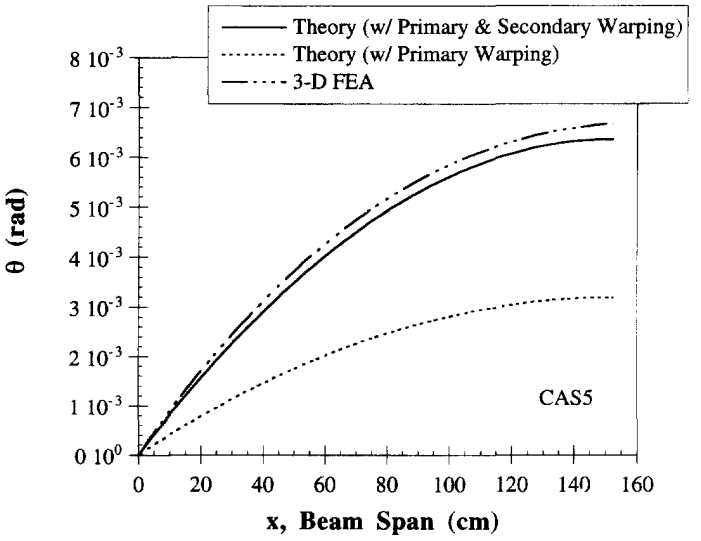

Fig. 28. Secondary warping effect on bending-induced twist for a CAS5 beam acted upon by 4.45 kN tip shear load.

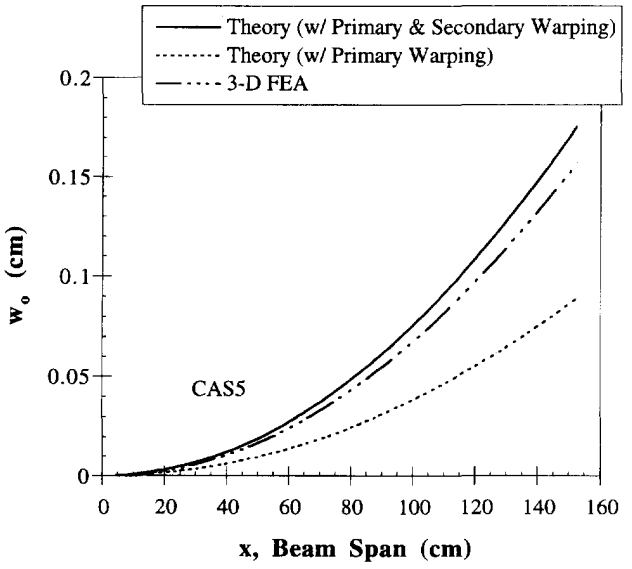

Fig. 29. Secondary warping effect on bending deflection for a CAS5 beam acted upon by 1.13 kN-m tip torque.

the other hand, secondary warping effects are significant for the coupled torsional behavior as shown in Fig. 28. Secondary torsional warping causes a 200% increase in twist at the free end.

Figures 29 and 30 show coupled bending and twist deflection of a thick CAS5 beam subjected to a 1.13 kN · m tip torque. Under this torsional loading, the influence of torsional secondary warping is large for the bending deformation as well as the twisting deformation. The above results reveal that the effects of secondary warping as well as primary warping are quite large for elastically tailored thick-walled composite beams.

CONCLUSIONS

An efficient and accurate anisotropic closed-section beam theory has been developed for both thin- and thick-walled composite beams. In this theory transverse shear effects, both of the cross-section and of the beam walls, are taken into account. Primary and

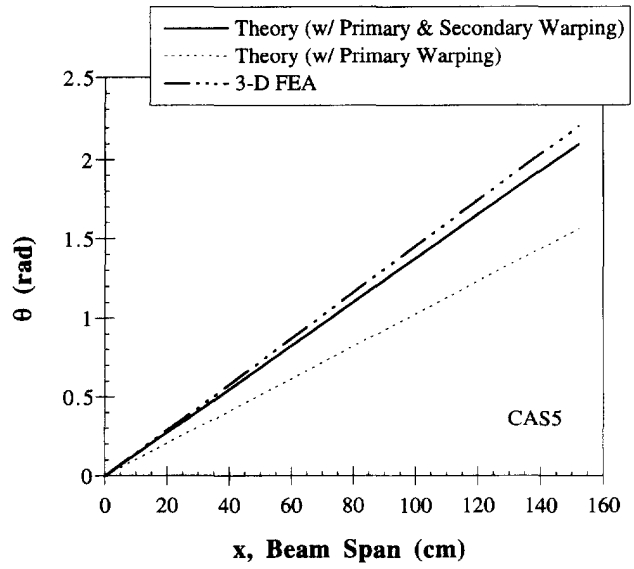

Fig. 30. Secondary warping effect on twist for a CAS5 beam acted upon by 1.13 kN-m tip torque.

secondary torsional warping was considered. The predictions of the present theory for thin-walled beam cases have been validated by comparison with available experimental data, other closed-form analysis, and refined beam finite element simulation. Good correlation between the present theory and other results was achieved. Three-dimensional finite element analyses have been performed for cantilevered thick-walled box beams under tip shear loading in an effort to validate the present theory for thick-walled beams. For these thick-walled beams no experimental, analytical, or numerical data was available. Again, the correlation between the predicted results from the present theory and 3-D FEA results was very good.

An efficient method to account for 3-D elastic effects was developed by incorporating refined stiffness coefficients. It has been shown that this method plays an important role in accurate predictions of twisting and coupled twisting deformations through correlations with many experimental and finite element results. The contribution of the secondary warping is small for a thin-walled box beam, however it becomes significant as the thickness of the beam wall increases. Both primary and secondary warping tend to decrease torsional and torsion-coupled beam stiffnesses and as a consequence, increases global deformations. The warping effects of laminated composite beams are known to be much greater than those for isotropic beams, especially for thick-walled beams. Accounting for secondary as well as primary warping in this case is critical to achieve accurate results.

REFERENCES

Atilgan, A. R., Hodges, D. H., Fulton, M. V. and Cesnik, C. E. S. (1991). Application of the variational-asymptotical method to static and dynamic behavior of elastic beams. In *Proc. 32nd AIAA/ASME/ASCE/AHS/ASC Structures, Structural Dynamics and Materials Conf.*, Baltimore, MD, 8–10 April, pp. 1078–1093.

Bauld, N. R., Jr. and Tzeng, L. S. (1984). A Vlasov theory for fiber-reinforced beams with thin-walled open cross sections. *Int. J. Solids Structures* **20,** 277–297.

Berdichevsky, V. L. (1982). On the energy of an elastic rod. *PMM* **45,** 518–529.

Berdichevsky, V. L., Armanios, E. and Badir, A. (1992). Theory of anisotropic thin-walled closed-cross-section beams. *Comp. Engng* **2,** 411–432.

Berdichevsky, V. L., Armanios, E. and Badir, A. (1993) A new look at thin-walled composite beam modeling approaches. In *Proc. 9th Int. Conf. on Composite Materials (ICCM/9)*, Madrid, Spain, 12–16 July, pp. 219–226.

Brunelle, E. J. (1972). Dynamical torsion theory of rods deduced from the equations of linear elasticity. *AIAA J.* **10,** 524–526.

Cesnik, C. E. S., Sutyrin, V. G. and Hodges, D. H. (1993). A refined composite beam theory based on the variational-asymptotical method. In *Proc. 34th AIAA/ASME/ASCE/AHS/ASC Structures, Structural Dynamics and Materials Conf.*, La Jolla, CA, 19–22 April, pp. 2710–2720.

Chandra, R., Stemple, A. D. and Chopra, I. (1990). Thin-walled composite beams under bending, torsional and extensional loads. *J. Aircraft* **27,** 619–626.
Chandra, R. and Chopra, I. (1992a). Experimental-theoretical investigation of the vibration characteristics of rotating composite box beams. *J. Aircraft* **29,** 657–664.
Chandra, R. and Chopra, I. (1992b). Structural response of composite beams and blades with elastic couplings. *Comp. Engng* **2,** 347–374.
Chandra, R. and Chopra, I. (1992c). Structural behavior of two-cell composite rotor blades with elastic couplings, *AIAA J.* **30,** 2914–2921.
Chang, S. I. and Libove, C. (1988). Shear flows, strains and rate of twist in single-cell thin-walled beams with anisotropic composite walls: Simple theory compared with NASTRAN and experiment. *ASME Winter Annual Meeting*, Chicago, IL, 27 November–2 December, pp. 49–70.
Hodges, D. H., Atilgan, A. R., Cesnik, C. E. S. and Fulton, M. V. (1992). On a simplified strain energy function for geometrically nonlinear behaviour of anisotropic beams. *Comp. Engng* **2,** 513–526.
Kim, C. and White, S. R. (1996). Analysis of thick hollow composite beams under general loadings. *Comp. Struct.*, **34,** 263–277.
Lekhnitskii, S. G. (1981). *Theory of elasticity of an anisotropic body*, English translation, Mir Publishers, Moscow.
Levinson, M. (1981). A new rectangular beam theory. *J. Sound Vibr.* **74,** 81–87.
Libove, C. (1988). Stresses and rate of twist in single-cell thin-walled beams with anisotropic walls. *AIAA J.* **26,** 1107–1118.
Librescu, L. and Song, O. (1991a). Behavior of thin-walled beams made of advanced composite materials and incorporating non-classical effects. *Apply. Mech. Rev.* **44,** S174–S180.
Librescu, L. and Song, O. (1991b). Free vibration and aeroelastic divergence of aircraft wings modeled as composite thin-walled beams. In *Proc. 32nd AIAA/ASME/ASCE/AHS/ASC Structures, Structural Dynamics and Materials Conf.*, Baltimore, MD, 8–10 April, pp. 2128–2136.
Librescu, L., Meirovitch, L. and Song, O. (1993). A refined structural model of composite aircraft wings for the enhancement of vibrational and aeroelastic response chacteristics. In *Proc. 34th AIAA/ASME/ASCE/AHS/ASC Structures, Structural Dynamics and Materials Conf.*, La Jolla, CA, 19–22 April, pp. 1967–1978.
Mansfield, E. H. and Sobey, A. J. (1979). The fiber composite helicopter blade, Part 1: Stiffness properties, Part 2: Prospects of aeroelastic tailoring. *Aeronaut. Q.* **30,** 413–449.
Mansfield, E. H. (1981). The stiffness of a two-cell anisotropic tube. *Aeronaut. Q.* **32,** 338–353.
Nixon, M. W. (1987). Extension-twist coupling of composite circular tubes with application to tilt rotor design. In *Proc. 28th AIAA/ASME/ASCE/AHS/ASC Structures, Structural Dynamics and Materials Conf.*, Monterey, CA, 6–10 April, pp. 295–303.
Pollock, G. D., Zak, A. R., Hilton, H. H. and Ahmad, M. F. (1994). Shear center for elastic thin-walled composite beams. *Int. J. Structural Engng and Mech.*, in press.
Rand, O. (1994). Free vibration of thin-walled composite blades. *Comp. Struct.* **28,** 169–180.
Reddy, J. N. (1984). A simple higher-order theory for laminated composite plates. *J. Appl. Mech.* **51,** 745–752.
Rehfield, L. W. (1985). Design analyses methodology for composite rotor blades. In *Proc. 7th Conf. on Fibrous Composites in Structural Design*, AFWAL-TR-85-3094, U.S. Air Force, pp. V(a)–V(a)-15.
Rehfield, L. W., Atilgan, A. R. and Hodges, D. H. (1990). Nonclassical behavior of thin-walled composite beams with closed cross sections. *J. Am. Helicopt. Soc.* **35,** 42–50.
Smith, E. C. and Chopra, I. (1991). Formulation and evaluation of an analytical model for composite box-beams. *J. Am. Helicopt. Soc.* **36,** 23–35.
Sokolnikoff, O. (1956). *Mathematical theory of elasticity*, McGraw-Hill, New York.
Song, O. and Librescu, L. (1993). Free vibration of anisotropic composite thin-walled beams of closed cross-section contour. *J. Sound Vibr.* **167,** 129–147.
Song, O. and Librescu, L. (1993). Dynamic refined theory of thin-walled beams of open-cross sections. *ASME Winter Annual Meeting*, New Orleans, LA, 28 November–3 December, pp. 233–240.
Stemple, A. D. and Lee, S. W. (1988). Finite element model for composite beams with arbitrary cross sectional warping. *AIAA J.* **26,** 1512–1520.
Subrahmanyam, K. B. (1993). Analysis of thin-walled composite beams by energy method. *J. Reinforced Plastics and Comp.* **12,** 642–669.
Sutyrin, V. G. and Hodges, D. H. (1995). On asymptotically correct plate theory. In *Proc. 36th AIAA/ASME/ASCE/AHS/ASC Structures, Structural Dynamics and Materials Conf.*, New Orleans, LA, 10–13 April, pp. 1800–1811.
Vinson, J. R. (1993). *The behavior of shells composed of isotropic and composite materials*, Kluwer Academic Publishers, Dordrecht.
Wu, X. X. and Sun, C. T. (1992). Simplified theory for composite thin-walled beams. *AIAA J.* **30,** 2945–2951.

APPENDIX

The stiffness matrix elements of composite box beams which appear in eqns (13) and (14) are:

$$K_{11} = \iint_f C_{11}\,\mathrm{d}y\,\mathrm{d}z + \iint_w C_{11}\,\mathrm{d}y\,\mathrm{d}z \tag{A1}$$

$$K_{12} = \iint_f C_{12}\left[1-4\left(\frac{y}{d}\right)^2\right]\mathrm{d}y\,\mathrm{d}z \tag{A2}$$

$$K_{13} = \iint_w C_{12}\left[1-4\left(\frac{z}{c}\right)^2\right]\mathrm{d}y\,\mathrm{d}z \tag{A3}$$

$$K_{14} = -\int\int_f C_{12}\left(\frac{\partial\psi}{\partial y}+z\right)dy\,dz-\int\int_w C_{12}\left(\frac{\partial\psi}{\partial z}-y\right)dy\,dz \tag{A4}$$

$$K_{21} = \int\int_f C_{12}\,dy\,dz \tag{A5}$$

$$K_{22} = \int\int_f C_{22}\left[1-4\left(\frac{y}{d}\right)^2\right]dy\,dz+\int\int_w C_{33}\left[1-4\left(\frac{y}{d}\right)^2\right]dy\,dz \tag{A6}$$

$$K_{25} = -\int\int_f C_{12}z\,dy\,dz \tag{A7}$$

$$K_{31} = \int\int_w C_{12}\,dy\,dz \tag{A8}$$

$$K_{33} = \int\int_f C_{33}\left[1-4\left(\frac{z}{c}\right)^2\right]dy\,dz+\int\int_w C_{22}\left[1-4\left(\frac{z}{c}\right)^2\right]dy\,dz \tag{A9}$$

$$K_{36} = -\int\int_w C_{12}y\,dy\,dz \tag{A10}$$

$$K_{41} = -\int\int_f C_{12}\left(\frac{\partial\psi}{\partial y}+z\right)dy\,dz-\int\int_w C_{12}\left(\frac{\partial\psi}{\partial z}-y\right)dy\,dz \tag{A11}$$

$$K_{44} = \int\int_f C_{33}\left(\frac{\partial\psi}{\partial z}-y\right)^2 dy\,dz+\int\int_f C_{22}\left(\frac{\partial\psi}{\partial y}+z\right)^2 dy\,dz+\int\int_w C_{22}\left(\frac{\partial\psi}{\partial z}-y\right)^2 dy\,dz+\int\int_w C_{33}\left(\frac{\partial\psi}{\partial y}+z\right)^2 dy\,dz \tag{A12}$$

$$K_{45} = \int\int_f C_{12}z\left(\frac{\partial\psi}{\partial y}+z\right)dy\,dz+\int\int_w C_{12}z\left(\frac{\partial\psi}{\partial z}-y\right)dy\,dz \tag{A13}$$

$$K_{46} = \int\int_f C_{12}y\left(\frac{\partial\psi}{\partial y}+z\right)dy\,dz+\int\int_w C_{12}y\left(\frac{\partial\psi}{\partial z}-y\right)dy\,dz \tag{A14}$$

$$K_{52} = -\int\int_f C_{12}z\left[1-4\left(\frac{y}{d}\right)^2\right]dy\,dz \tag{C15}$$

$$k_{54} = \int\int_f C_{12}z\left(\frac{\partial\psi}{\partial y}+z\right)dy\,dz+\int\int_w C_{12}z\left(\frac{\partial\psi}{\partial z}-y\right)dy\,dz \tag{A15}$$

$$K_{55} = \int\int_f C_{11}z^2\,dy\,dz+\int\int_w C_{11}z^2\,dy\,dz \tag{A16}$$

$$K_{63} = -\int\int_w C_{12}y\left[1-4\left(\frac{z}{c}\right)^2\right]dy\,dz \tag{A17}$$

$$K_{64} = \int\int_f C_{12}y\left(\frac{\partial\psi}{\partial y}+z\right)dy\,dz+\int\int_w C_{12}y\left(\frac{\partial\psi}{\partial z}-y\right)dy\,dz \tag{A18}$$

$$K_{65} = \int\int_f C_{11}yz\,dy\,dz+\int\int_w C_{11}yz\,dy\,dz \tag{A19}$$

$$K_{56} = \int\int_f C_{11}y^2\,dy\,dz+\int\int_w C_{11}y^2\,dy\,dz \tag{A20}$$

where f and w denote flange and web, respectively.